NISTIR 6519

Effect of Drying Shrinkage Cracks and Flexural Cracks on Concrete Bulk Permeability

Kenneth A. Snyder

National Institute of Standards and Technology
Technology Administration
U.S. Department of Commerce

NISTIR 6519

Effect of Drying Shrinkage Cracks and Flexural Cracks on Concrete Bulk Permeability

Kenneth A. Snyder
Building Materials Division
Building and Fire Research Laboratory
National Institute of Standards and Technology
Gaithersburg, MD 20899-8621

Sponsor:
U.S. Nuclear Regulatory Commission

May 2000

U.S. DEPARTMENT OF COMMERCE
William M. Daley, Secretary

TECHNOLOGY ADMINISTRATION
Dr. Cheryl L. Shavers, Under Secretary
of Commerce for Technology

NATIONAL INSTITUTE OF STANDARDS AND TECHNOLOGY
Raymond G. Kammer, Director

Abstract

A review of the computer program `4sight` has revealed that an accurate prediction of water transport through the concrete depends upon an accurate prediction of the crack formation within the concrete. A model for predicting both the width and the spacing of flexural and drying shrinkage cracks is employed. The results are used to estimate the composite concrete permeability. A deterministic structural analysis is performed to demonstrate the procedure. The analysis is repeated using a Monte Carlo approach in order to assess the effects of input parameter variability.

The principles outlined in this report will be incorporated into the `4sight` computer program. The prediction of shrinkage and flexural crack width and crack spacing will allow the user to consider the effects of various concrete mixture designs. The mean values reported will assist the user in determining which factors have the greatest effect on the expected crack width and crack spacing. The reported uncertainties will help the user assess the maximum statistical variation allowed for critical concrete mixture and structural design parameters.

Keywords: building technology; concrete; cracking; nuclear disposal; permeability; reinforced concrete; restrained shrinkage

Contents

List of Tables

List of Figures

1 Introduction

A recent review [1] of the `4sight` computer model [2] revealed that the most important factor in affecting ionic transport through concrete is the presence of cracks. The presence of cracks not only controls the quantity of ions transported, but can also control whether there will be any convective transport at all.

Cracking can originate within the concrete due to a number of mechanisms. During the placement of the concrete, if the evaporation rate is great enough, the concrete surface can develop tensile stresses sufficient to crack the plastic concrete. These *plastic shrinkage cracks* typically extend through the section of the concrete. If during placement the concrete member experiences settlement, and the concrete has insufficient strength to withstand the resulting stresses, the concrete will undergo *settlement cracking*. If the concrete member is a slab that spans a distance, the concrete surface in tension (typically the bottom surface) will possibly develop *flexural cracks* after removal of the concrete form work. During the cement paste hydration, a large portion of the initial mix water will be consumed, with the generation of heat. Differences between concrete temperature and ambient temperature can lead to *thermal cracking*, depending on the mechanical state of the concrete. The continued removal of water by the hydration process will generate a chemical shrinkage stress that can initiate *autogeneous shrinkage cracks*. Subsequent drying due to ambient conditions will also generate a shrinkage stress that can initiate *drying shrinkage cracks*.

Some cracks are to be expected, while others are the result of construction practices. Plastic shrinkage cracking, thermal cracking, and settlement cracking can be either avoided or minimized by following industry guidelines (ACI Manual of Concrete Practice) for the placement and curing of concrete. Both flexural cracks and shrinkage cracks are to be expected (under the assumptions given above), and the resulting crack widths and spacings can be predicted. Therefore, the incorporation of crack modeling by `4sight` will be limited to the prediction of flexural and shrinkage cracking and their effect on transport.

The models for the crack width and spacing described here will be implemented into a structural analysis of a vault that is meant to represent a typical design. Under ideal conditions, a structural engineer will perform an analysis of the specific vault in question, and then input the calculated parameters into `4sight`. The structural analysis presented is not meant to represent an exhaustive analysis. However, it is the default analysis that will be performed in the absence of any such analysis on the part of the engineer who is using `4sight`.

2 Structural Model

In order to proceed, one must reasonably estimate the geometry of a representative vault structure. The principles used here for estimating the composite permeability due to cracking are general enough to apply to many different vault designs. A general geometry

and construction plan for the vault will be assumed here for the purpose of illustrating the analysis.

2.1 Vault Geometry

To partially simplify the structural analysis, the vault will be approximated by a container with horizontal dimensions L_1 and L_2 such that their ratio is greater than two: $L_1/L_2 > 2$. The corresponding edge loads f_1 and f_2 have a quartic dependence on length [3]:

$$\frac{f_1}{f_2} = \frac{L_2^4}{L_1^4} \tag{1}$$

Since the load on the shorter span is 16 times greater, the vault analysis will be performed using one-way slab design.

2.2 Structural Joints

The formation of both shrinkage and flexural cracks depends strongly on the amount and the location of the steel reinforcement. In addition, the positive moment due to the load will depend on how the roof is attached to the vault walls. The roof could either rest on the walls (simply supported) or it could be rigidly attached to the walls (continuous reinforcement). For a given geometry and load, the simply supported roof will subjected to approximately twice the positive moment.

Although a design that assumes a simply supported roof would be more conservative, it is quite unlikely that this would occur in practice. By definition, a simply supported roof must be able to move freely over the vault walls. While this type of construction can eliminate shrinkage cracks, the joint provides a likely path for the ingress of fluids and ionic species. Therefore, a continuously reinforced design is used.

In addition to the analysis of the flexural and shrinkage crack formation at the center of the roof, there will exist negative moments at the joints between the roof and the walls. Although an analysis of these cracks is not performed here, the method for incorporating these cracked sections into the overall composite properties follows from the positive moment analysis. In addition, no analysis of the shear stress at the joint between the roof and the wall is presented.

2.3 Roof Construction

The scenario adopted here is that the vault will first be filled with waste materials, compacted, and the roof cast in place on top of the vault contents. The expected thickness of the vault roof is assumed to be 1 m, and the contents of the vault will probably settle under the dead load of the roof and the soil above the vault. The roof will then flex, possibly forming flexural cracks. In fact, a small amount of flexure will be useful in that it will help close shrinkage cracks at the top surface.

3 Cracked Composite Model

Given the construction plan outlined above, the concrete roof will likely experience shrinkage stresses during the first months, and later experience flexural stresses as the vault contents settle over time. While the flexural stresses will widen the shrinkage cracks on the bottom of the roof, they will contract the shrinkage cracks on the top surface of the vault. The composite material containing both shrinkage and flexural cracks will then have a permeability that is greater than the uncracked concrete.

3.1 Crack Geometry

For simplicity, the cracks are approximated by plane parallel walls separated by the observed crack width. The open cracks on the tension face of the roof propagate upwards to the neutral axis. While the depth of crack penetration is accurate, the approximation of the cracks by plane parallel walls is conservative. This assumption does not account for either the "V" shape of the crack or the crack wall surface roughness, both of which would act to reduce the crack permeability with respect to one with plane parallel sides.

The permeability k' of a crack with plane parallel sides is solely a function of the crack width w:

$$k' = \frac{w^2}{12} \tag{2}$$

The derivation is given in Appendix A.

3.2 Composite Permeability

The composite model for the roof bulk permeability is shown in Fig. 1. The cracks propagate from the bottom of the slab up to the neutral axis. The thickness of the slab is h, and the depth to the neutral axis is expressed as the product αh. The permeability of the uncracked concrete is k_c. The composite has an additional component with permeability k' due to m cracks, each with width w, over the entire span L. For Fig. 1(a), the permeability k_b of the two bottom sections k_c and k' in parallel is a weighted average:

$$k_b = \frac{1}{L}\left[(L - m_1 w_1)\, k_c + m_1 w_1 k'\right] \tag{3}$$

The composite permeability k^* of k_b and k_c (top section in Fig. 1(a)) in series is treated like the corresponding problem of conductors in series:

$$\begin{aligned} \frac{1}{k^*} &= \frac{\alpha}{k_c} + \frac{1-\alpha}{k_b} \\ k^* &= \frac{k_c k_b}{(1-\alpha)k_c + \alpha k_b} \end{aligned} \tag{4}$$

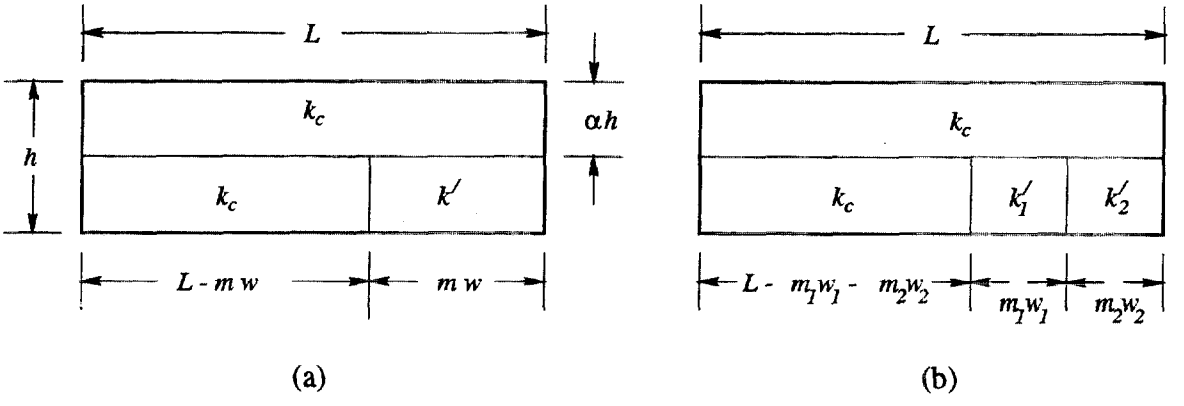

Figure 1: Composite design for the bulk roof design for uncracked permeability k_c and crack permeability k': (a) cracks with a single width and spacing; (b) two different crack widths and crack spacings.

Given that a crack with a width of one micrometer has a permeability of 8×10^{-14} m^2, and that concrete permeability is on the order of 10^{-18} m^2, this equation can be simplified:

$$k^*(k_b \gg k_c) = \frac{k_c}{\alpha} \tag{5}$$

Therefore, for a given concrete mixture, the control of roof permeability is the control of the neutral axis depth, given that there is sufficient flexural strain to close shrinkage cracks at the top surface of the roof.

The relationship between composite permeability and the neutral axis depth should not be used as means to reduce vault permeability. Within practical limits, the depth of the neutral axis can only affect the composite permeability by a factor of two or three. However, variations in concrete mixture proportions, and cementitious materials, can change the concrete permeability by a factor of 10 to 100. Therefore, efforts to reduce overall permeability should concentrate on controlling the concrete mixture.

3.3 Composite Crack Model

The way in which the effects of the shrinkage and flexural cracks are combined depends upon the formation and the geometry of the cracks. The shrinkage cracks will likely form first, and there will be a number m_s of these cracks, each with width w_s, separated by a distance L_s. Similarly for the flexural cracks, formed independently of the shrinkage cracks, there will be m_f flexural cracks, each with width w_f, separated by a distance

L_f. The objective is to consider the formation of the cracks independently, and then determine the properties of the cracked material.

The resulting width and separation of cracks depends on the cracking scenario. Here, the assumption is that the shrinkage cracks form first and the flexural cracks form after the vault contents settle. For the case when the crack spacings are approximately equal, so that $L_s \approx L_f$, the later flexural cracks should simply widen the existing shrinkage cracks. If $L_s \ll L_f$, the flexure should once again widen the existing shrinkage cracks. For the third case when $L_s \gg L_f$, new flexural cracks should form in between the existing shrinkage cracks, each with width w_f and separated by L_f. If one assumes that the existing shrinkage cracks contribute to the flexural cracking, the shrinkage cracks should also widen by an amount equal to w_f.

The particular crack model to choose from in Fig. 1 depends upon the ratio L_s/L_f. For the first two scenarios presented ($L_s/L_f \approx 1, L_s/L_f \ll 1$), the flexural stress widens the existing shrinkage cracks. Each crack will then have the same width and spacing, corresponding to the model shown in Fig. 1(a). For the third case ($L_s/L_f \gg 1$), there will exist two crack widths and spacings. The existing shrinkage cracks will widen by an amount w_f, and the $m_f - m_s$ flexural cracks will each have a width w_f, corresponding to the model shown in Fig. 1(b). The analysis of this ternary composite bulk permeability k^* follows from the binary example given previously. The parameters for each model are shown in Table 1.

Table 1: Parameters for the composite permeability calculation for m cracks of width w. The crack model refers to that shown in either Fig. 1(a) or Fig. 1(b).

L_s/L_f	Model	w_1'	m_1'	w_2'	m_2'
< 1	(a)	$w_s + \frac{m_f}{m_s} w_f$	m_s		
≈ 1	(a)	$w_s + w_f$	m_s		
> 1	(b)	$w_s + w_f$	m_s	w_f	$m_f - m_s$

4 Flexural Crack Model

The model for estimating flexural crack widths and spacings is based upon the recommendations given in ACI 224.2R-90 [4]. The recommendation for estimating flexural crack width w_f is the Gergely-Lutz equation:

$$w_f = 2.2\,\beta\,\epsilon_r\,(d_c A_n)^{1/3} \tag{6}$$

The definitions of the parameters are as follows:

d_1 : distance from the neutral axis to the tension face
d_2 : distance from the neutral axis to the centroid of the tension steel reinforcement
β : the ratio d_1/d_2
ϵ_r : strain in the tension steel reinforcement
d_c : minimum concrete cover thickness, measured to center of tension reinforcement
A_n : the largest area of concrete, perpendicular to the reinforcement, symmetric about the centroid of the tension reinforcement, divided by the number of bars

The estimate of the spacing between flexural cracks is based upon the CEB/FIP model. The maximum distance l_s over which slip can occur can be approximated from the following equation:

$$l_s = \frac{d_r}{3.6\, p_s} \tag{7}$$

The quantity d_r is the steel reinforcement diameter, and p_s is the area of steel divided by the effective area of concrete in tension. The average spacing between flexural cracks L_f is taken to be 2/3 this value:

$$L_f = \frac{d_r}{5.4\, p_s} \tag{8}$$

5 Shrinkage Cracks Model

The drying shrinkage model is based upon the calculations of Base and Murray [5] for calculating the width w_s and spacing L_s of shrinkage cracks. The model requires the following design parameters:

L : length of slab
E_s : Young's modulus of the steel reinforcement
E_c : Young's modulus of the concrete
n : modulus ratio - E_s/E_c
A_s : total area of steel in cross section
A_c : total area of concrete in cross section
p : reinforcement ratio - A_s/A_c
d_r : steel reinforcement bar diameter
ϵ_{sh} : shrinkage strain
ϵ_t : concrete tensile strain at crack initiation

The "no-bond" length a of reinforcement near a crack can be approximated from the reinforcement diameter d_r and the reinforcement ratio p:

$$a = 0.08 \frac{d_r}{p} \tag{9}$$

The number of shrinkage cracks m_s that form along a slab of length L can be estimated from the following equation:

$$m_s = 1 + \frac{Lnp}{2a}\left[\frac{\epsilon_{sh} - \epsilon_t}{3\,\epsilon_t}\right] \tag{10}$$

The result is used to calculate the steel stress f_s:

$$f_s = E_s\left(\frac{\epsilon_{sh} + 2\epsilon_t}{3}\right)\left(\frac{L - 2ma}{npL + 2ma}\right) \tag{11}$$

Finally, the average shrinkage crack width w_s can be estimated from the following equation:

$$w_s = 2a\left(\frac{f_s}{E_s} + \frac{\epsilon_{sh}}{3}\right) \tag{12}$$

6 Design Example

The following design analysis starts from the concrete mixture design and proceeds to estimates of the composite permeability.

6.1 Mixture Design

The mixture design chosen for this example was meant to be a balance between quality of concrete and ease of formulation and placement. The design compressive strength f'_c is 35 MPa, which is within the normal strength guidelines of ACI 211.

The constituent material properties are as follows:

Cement Type	Type I
Cement Density	3.2 g/cm^3
CA Density	2.8 g/cm^3
CA Moisture	3 %
FA Density	2.6 g/cm^3
FA Moisture	2 %
Max. Agg. Diameter	25 mm

The percentages given for moisture content are on a mass basis.

For a reinforced foundation with a design strength of 35 MPa, ACI 211 recommends the following mixture design:

Constituent	Mass (kg/m^3)
Water	190
Cement	399
Coarse Agg.	1104
Fine Agg.	757

A high range water reducer is not specified, simplifying the formulation.

6.2 Concrete Properties

This proposed mixture design has the following expected properties:

w/c	0.43
Slump	76 mm
Air Content	1.5 %
Concrete Density	2450 kg/m^3
Specific Heat	1.05 J/g °C
28 day Heat Release	66 J/g

6.2.1 Young's Modulus

The equation for estimating the Young's modulus is described in Nilson [3]:

$$E_c = \left(3320\,[\mathrm{MPa}^{1/2}]\sqrt{f'_c} + 6890\,[\mathrm{MPa}]\right)\left(\frac{\rho_c}{2330\,[\mathrm{kg/m^3}]}\right)^{1.5} \tag{13}$$

This equations can be applied to normal density concretes over a wide range of design strengths: 21 MPa $\leq f'_c \leq$ 83 MPa.

For the mixture given above, the estimated Young's modulus is 28.6 GPa.

6.2.2 Modulus of Rupture

A concrete member in tension will experience a tensile stress f_t. In flexure, the member will remain uncracked until the tensile stresses exceed the modulus of rupture. The approximation for the modulus of rupture is taken from Nilson [3]:

$$0.67\,[\mathrm{MPa}^{1/2}]\sqrt{f'_c} \leq f_r \leq 1.0\,[\mathrm{MPa}^{1/2}]\sqrt{f'_c}$$

The mixture design used here yields the following result:

$$4.0\,\mathrm{MPa} \leq f_r \leq 5.9\,\mathrm{MPa}$$

6.2.3 Drying Shrinkage

The ACI guideline for estimating the ultimate drying shrinkage strain $\epsilon_{s,u}$ is shown in Fig. 2(a) as a function of the mixture design water content. For this mixture, the expected ultimate drying shrinkage is approximately 600 μm/m. Reducing this value requires lowering the water content of the concrete mixture. To do this at constant strength requires increasing the maximum aggregate size, which will reduce the overall water demand.

The expected shrinkage strain ϵ_s will be less than the ultimate value due to mitigating factors. ACI 209R-82 gives the following mathematical expression for the effect each factor has on the expected shrinkage strain:

$$\epsilon_s = \epsilon_{s,u} \prod_i \gamma_i \tag{14}$$

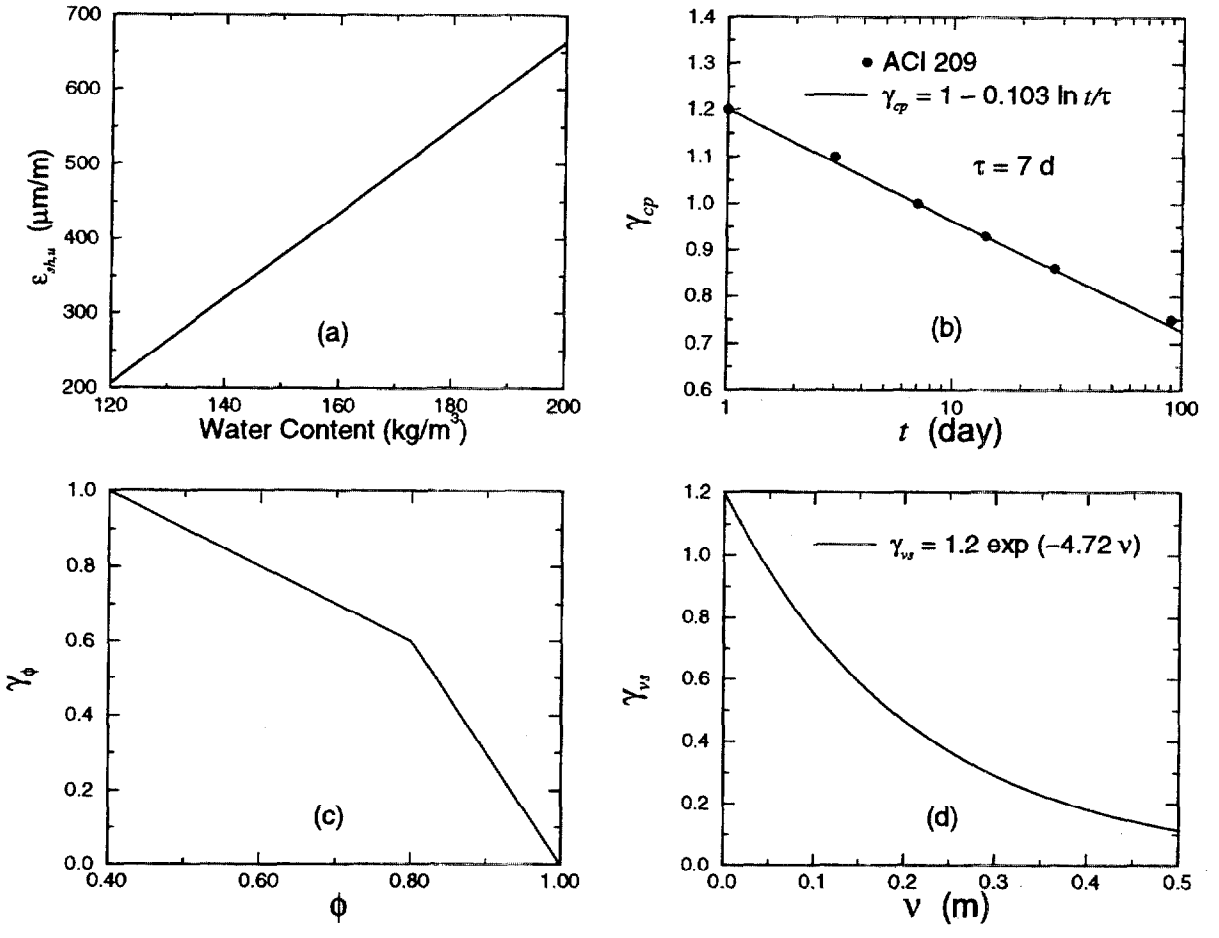

Figure 2: Quantities for estimating shrinkage strain: (a) ultimate drying shrinkage strain; (b) duration of moist curing; (c) ambient relative humidity; and (d) volume-to-surface ratio.

There are three factors γ_i considered here: duration of curing γ_{cp}; ambient relative humidity γ_ϕ; and volume-to-surface ratio γ_{vs}. There are other factors outlined in ACI 209, but the factors relating to concrete mixture design do not apply here since we are using the ultimate drying shrinkage prediction shown in Fig. 2(a).

The factor γ_{cp} for the duration of moist curing is shown in Fig. 2(b) as a function of curing time t. The filled circles are the recommendations from ACI 209, and the curve is an approximation:

$$\gamma_{cp} = 1 - 0.103 \ln\left(\frac{t}{\tau}\right) \tag{15}$$

The value of τ is 7 d. Since moist curing for 7 days is typical, the corresponding value of γ_{cp} is one, and so it will have little effect on the overall expected shrinkage strain for this problem.

The factor γ_ϕ for the ambient environment is shown in Fig. 2(c) as a function relative humidity ϕ. Over the range of relative humidity shown in Fig. 2(c), the factor has two linear regions:

$$\gamma_\phi = \begin{cases} 1.4 - 1.0\,\phi & 0.40 \le \phi \le 0.80 \\ \\ 3.0 - 3.0\,\phi & 0.80 \le \phi \le 1.00 \end{cases} \tag{16}$$

It is difficult to estimate the ambient relative humidity for a buried vault. However, most certainly the relative humidity will be greater than 40 % and less than 100 %. As a conservative estimate, the factor γ_ϕ will be assigned a value of one here. However, in practice, an assessment should use a value commensurate with the specific soil conditions being considered.

The factor γ_{vs} for vault geometry is shown in Fig. 2(d) as a function of the volume-to-surface ratio ν. ACI 209 expresses this factor in analytic form:

$$\gamma_{vs} = 1.2\,\exp\left(-\nu/\nu_o\right) \tag{17}$$

The quantity ν_o equals 0.212 m, and simply rescales ν. For the present design, the length and width of the slab are L and $2L$, respectively. For a slab thickness h, the volume-to-surface ratio ν is the following:

$$\nu = \frac{h}{2 + 3\frac{h}{L}} \tag{18}$$

For a slab thickness h equal to 1 m, and a slab length L equal to 10 m, the volume-to-surface ratio ν equals 0.435, corresponding to a shrinkage factor γ_{vs} of 0.15.

The expected shrinkage strain ϵ_{sh} is the product of the ultimate shrinkage strain $\epsilon_{sh,u}$ and the factors γ_i:

$$\begin{aligned} \epsilon_{sh} &= \epsilon_{sh,u}\,\gamma_{cp}\,\gamma_\phi\,\gamma_{vs} \\ &= 90\ \mu\text{m/m} \end{aligned} \tag{19}$$

This is significantly less than the 600 μm/m based solely on the concrete mixture water content.

6.3 Steel Properties

The steel considered for this example is ASTM A 615 Grade 60 steel; a steel with a 60 000 psi yield strength. The corresponding properties in SI are as follows:

$$\begin{aligned} E_s &= 200\,\text{GPa} \\ f_y &= 414\,\text{MPa} \end{aligned} \tag{20}$$

Therefore, the modulus ratio n, defined as E_s/E_c, is approximately 7.

6.4 Reinforcement Ratio Requirements

There is a limit on both the minimum and maximum amount of steel reinforcement allowed in the design. The minimum limit is intuitive from a structural standpoint. The maximum limit is determined by the ultimate failure mode.

The two regions of stress within the slab are the tension zone in the bottom and the compression zone in the top. At the ultimate load, either the steel will fail in tension, or the concrete will fail in compression. Steel failure in tension is a gradual process, giving "warning" of impending failure. Compressive failure, by contrast, is a sudden mode of failure. Therefore, there is a maximum limit on the amount of steel reinforcement so as to insure that the steel will yield before the concrete fails in compression.

The amount of steel at which the two modes of failure coincide at ultimate load is the balanced reinforcement ratio p_b:

$$\begin{aligned} p_b &= \frac{f'_c}{f_y} \frac{0.85\beta}{1 + \frac{f_y}{600\,[\mathrm{MPa}]}} \\ &= 0.033 \end{aligned} \tag{21}$$

For a 35 MPa concrete mixture, the recommended value of β is approximately 0.775.

The maximum allowable reinforcement ratio p_{max} is 3/4 the balance reinforcement ratio:

$$\begin{aligned} p_{max} &= 0.75\, p_b \\ &= 0.025 \end{aligned} \tag{22}$$

The minimum reinforcement ratio p_{min} can be calculated based on the assumption that a steel stress f_s of 2/3 the yield stress is an acceptable limit of steel stress immediately after cracking. The corresponding reinforcement is the following:

$$\begin{aligned} p_{min} &= \frac{0.220\,[\mathrm{MPa}^{1/2}]\sqrt{f'_c}}{f_y} \\ &= 0.0031 \end{aligned} \tag{23}$$

This is in agreement with the ACI recommendation:

$$\begin{aligned} p_{min} &= \frac{1.38\,[\mathrm{MPa}]}{f_y} \\ &= 0.0033 \end{aligned} \tag{24}$$

6.5 Roof Geometry

The dimensions of the roof slab are defined in Fig. 3 and are given the following values:

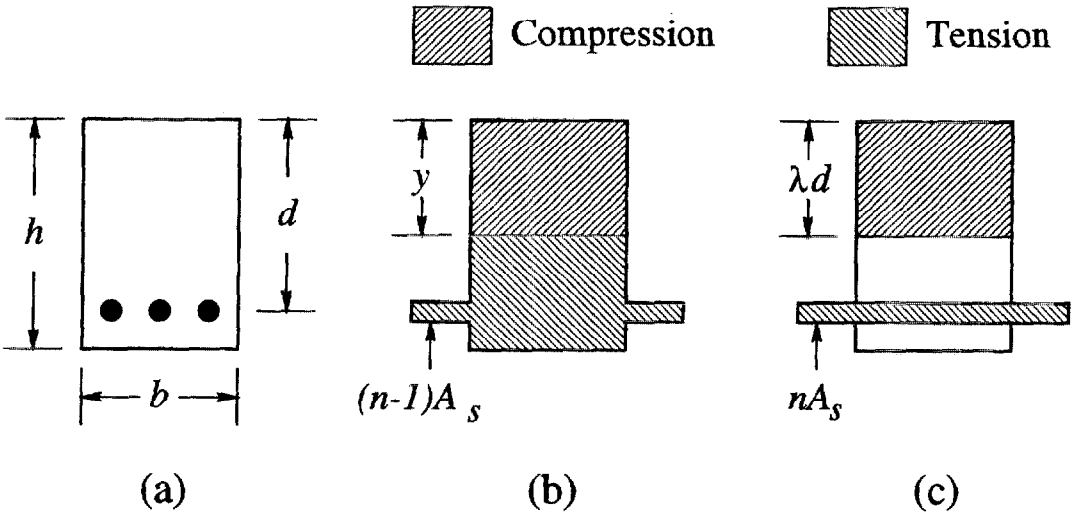

Figure 3: Roof geometry used for analysis: (a) original cross section showing location of steel reinforcement (filled circles); (b) transformed section used for uncracked analysis; (c) transformed section used for cracked analysis.

$$
\begin{aligned}
h &: 1.0 \text{ m} \\
d &: 0.9 \text{ m} \\
b &: 1.0 \text{ m} \\
d_r &: 35.8 \text{ mm}
\end{aligned}
$$

The slab width b is set to 1.0 m to simplify the analysis by normalizing values on a "per meter" basis. The reinforcement diameter d_r of 35.8 mm corresponds to a No. 11 bar.

6.6 Positive Moment

The positive moment at the center of the roof slab is determined from the dead load due to the concrete mass and the mass of soil above the vault. The thickness h of the concrete roof is 1 m, and the assumed thickness of soil h_s over the roof is 10 m. The density of the concrete ρ_c is 2450 kg/m^3, and the density of the soil ρ_s is assumed to be 1500 kg/m^3. The nominal uniform load (pressure) w_n on the roof depends upon the thickness of each element:

$$
\begin{aligned}
w_n &= \rho_c g h + \rho_s g h_s \\
&= 171,000 \,\text{N/m}^2
\end{aligned}
\tag{25}
$$

The quantity g is the gravitational acceleration (9.8 m/s^2). The moment due to the load requires an estimated ultimate load w_u:

$$
\begin{aligned}
w_u &= 1.4\, w_n \\
&= 239,000 \,\text{N/m}^2
\end{aligned}
\tag{26}
$$

The quantity 1.4 is a margin of safety for dead loads.

The positive moment M_+ at mid-span due to the ultimate load w_u is the integral of the load over half the span:

$$\begin{aligned} M_+ &= \theta \int_0^b \int_0^{L/2} r w_u \, dr \, db \\ &= \theta b \frac{w_u L^2}{8} \end{aligned} \tag{27}$$

The quantity θ is a factor that depends on the construction type. For a simply supported slab, $\theta = 1$. For an end span that is restrained at the discontinuous end, $\theta = 4/7$, as is used here:

$$M_+ = 1,707,000 \text{ N m}$$

6.7 Uncracked Analysis

The starting point for the structural analysis begins with an analysis of the roof assuming that there are neither flexural nor shrinkage cracks. The design loads can then be compared to the modulus of rupture. If the design loads are greater than the modulus of rupture, the analysis must be repeated assuming flexural cracking.

6.7.1 Neutral Axis

As the slab flexes, the top portion of the roof will be in compression, and the bottom portion in tension. There will exist a 2-D surface through the midsection of the slab that defines where the concrete is neither in tension nor in compression. This surface is referred to as the neutral axis.

For linear elastic media, a member in flexure will have strains that are linearly proportional to the distance from the neutral axis. Since the coefficient of proportionality is same for both the tensile and the compressive strains, the location of the neutral axis can be determine by balancing the moments of the slab cross section.

To simplify the calculation of the tensile and compressive moments, the concrete slab cross section is first transformed into an equivalent cross section. Specifically, the steel is replaced mathematically by an area of concrete equal to $(n-1)A_s$, and located at the depth of the reinforcement. This is shown schematically in Fig. 3(b) for this analysis.

The equation for calculating the moment is the integral of the moment arm r (absolute distance from the neutral axis) over the slab cross section ($da = dr\,db$):

$$M = \int r \, da \tag{28}$$

The moment above the neutral axis, which is located at depth y from the top of the slab, is set equal to the moment below the neutral axis:

$$\frac{by^2}{2} = \frac{b\,(h-y)^2}{2} + (d-y)\,(n-1)\,A_s \tag{29}$$

The quadratic terms in y cancel, yielding an algebraic solution:

$$y = \frac{bh^2 + 2(n-1)A_s d}{2bh + 2(n-1)A_s} \tag{30}$$

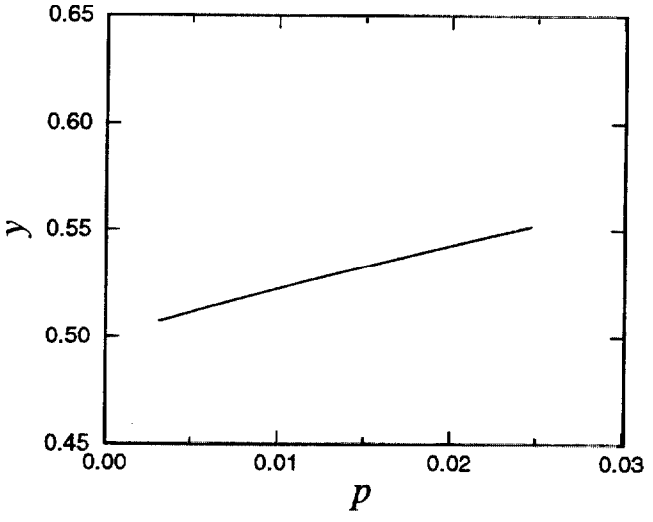

Figure 4: Depth of neutral axis y as a function of the reinforcement ratio p for the uncracked analysis.

The steel area can be expressed as a function of the steel reinforcement ratio p:

$$p = \frac{A_s}{A_c} = \frac{A_s}{bh} \tag{31}$$

This can be used to simplify the equation for y:

$$y = \frac{h}{2}\left[\frac{1 + 2(n-1)pd/h}{1 + (n-1)p}\right] \tag{32}$$

The neutral axis depth y, as a function of the reinforcement ratio p, is shown in Fig. 4. For the uncracked analysis, the depth appears to be insensitive to the reinforcement ratio.

6.7.2 Concrete and Steel Stresses

The stresses within the concrete section will depend upon the moment of inertia I of the slab. The moment of inertia is the integral of the square of the moment arm over the slab cross section:

$$I = \int r^2 \, da \tag{33}$$

For the transformed section, the moment of inertia is

$$I = \frac{by^3}{3} + \frac{b(h-y)^3}{3} + (d-y)^2\,(n-1)A_s \tag{34}$$

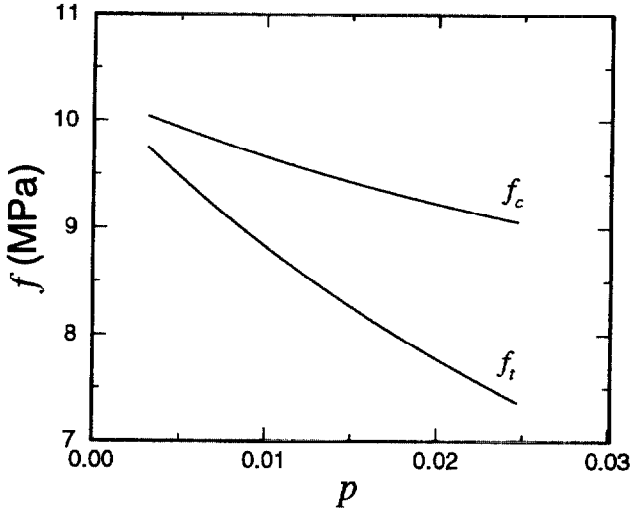

Figure 5: Compressive stress f_c and tensile stress f_t for the uncracked analysis.

The stress at the compression f_c and tension f_t surfaces are proportional to their distance from the neutral axis:

$$f_c = M_+ \frac{y}{I} \qquad\qquad f_t = M_+ \frac{h-y}{I} \tag{35}$$

These quantities are shown in Fig. 5 as a function of the reinforcement ratio p. The compressive stress f_c is approximately one-quarter the design strength f'_c for all values of the reinforcement ratio. However, the tensile stress f_t is considerably greater than the estimated modulus of rupture range of 4 MPa to 6 MPa. Therefore, one expects that the roof slab would develop cracks in the portion of the concrete that is in tension.

6.8 Cracked Section Analysis

Based upon the previous analysis, it is likely that the concrete roof slab will crack due to flexural loading. These cracks will initiate at the tension surface and continue upward to approximately the neutral axis. Analysis based upon this idea requires a different transformed cross section. This transformed cross section is similar to that of the uncracked transformed cross section with the one exception that the concrete below the neutral axis is disregarded in the analysis.

6.8.1 Neutral Axis

Determination of the neutral axis for the cracked cross section is similar to the uncracked case. However, one assumes that the concrete in tension does not contribute to the moment calculation. This transformed section, similar to that used for the uncracked analysis, is shown schematically in Fig. 3(c). The portion of the concrete below the neutral axis does not contribute to the analysis, and the steel has been transformed into an area nA_s of concrete.

Let the depth of the neutral axis be a fraction λ of the reinforcement depth d. The balance of moments occurs between the concrete in compression and the steel tension:

$$b\frac{(\lambda d)^2}{2} = nA_s(d - \lambda d) \tag{36}$$

The solution for λ is found from the quadratic equation:

$$\lambda = \sqrt{(np)^2 + 2np} - np \tag{37}$$

The neutral axis depth factor λ is shown in Fig. 6(a) as a function of the reinforcement ratio p. In contrast to the uncracked section analysis, the depth of the neutral axis for the cracked cross section has a strong dependence on the reinforcement ratio.

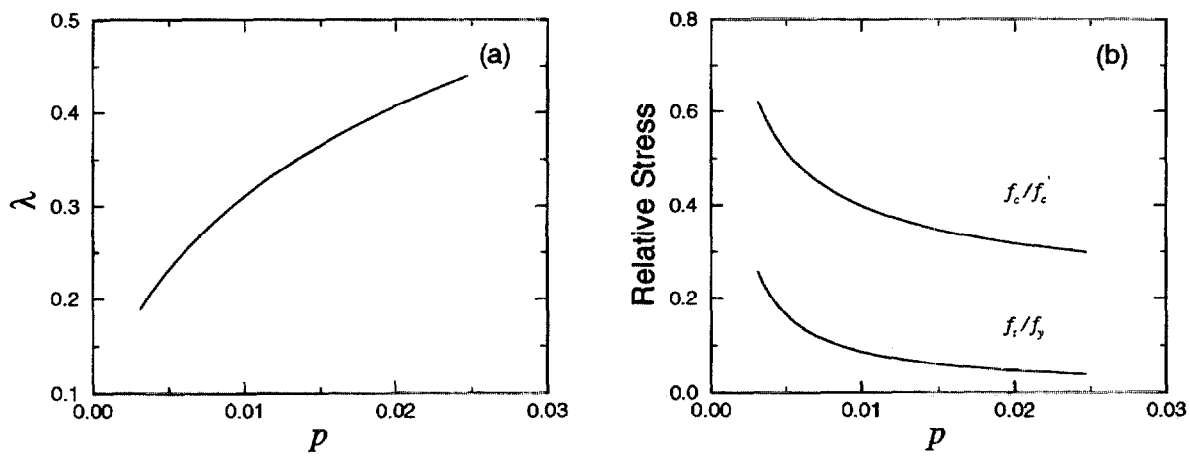

Figure 6: Analysis results: (a) Relative depth of neutral axis λ; (b) Relative tensile stress f_t/f_y and compressive stress f_c/f_c' for the cracked section analysis.

6.8.2 Concrete Stress

The stresses at the compression surface and the steel reinforcement are calculated in much the same way as for the uncracked analysis. The moment of inertia calculation omits the

second term due to the concrete in tension. The compressive stress f_c in concrete at the top surface and the tensile stress f_t in the steel are proportional to their distance from the neutral axis:

$$f_c = M\frac{d\lambda}{I} \qquad f_t = M\frac{d(1-\lambda)}{I} \tag{38}$$

The compressive stress f_c and the tensile stress f_t are shown in Fig. 6(b) as a function of the reinforcement ratio p. Further, both stresses are normalized by their ultimate values. The ultimate compressive stress is f'_c, and the ultimate tensile stress is the steel yield stress f_y.

Although the tensile stress is greater than the compressive stress, the relative tensile stress is less. Noting that one can assume linear elastic behavior for $f_c/f'_c < 0.50$, the design thus far is relatively close to this limiting value. Therefore, for this design, a slab thickness of less than 1 m would be inadvisable since that would increase the ratio f_c/f'_c because the majority of the load w_u is due to the soil above the vault.

6.8.3 Concrete Strain

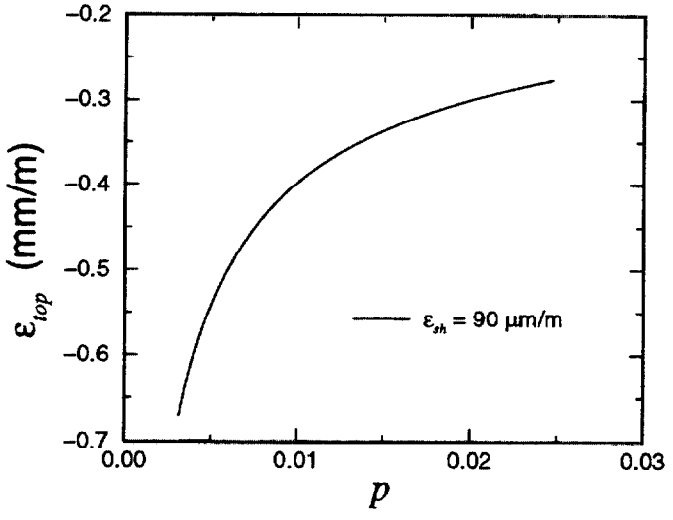

Figure 7: Strain in top surface of the slab for drying shrinkage strain $\epsilon_{sh} = 90$ μm/m.

The strain at the top surface of the vault can be estimated from the flexural stress and the expected shrinkage strain ϵ_{sh}. The flexural strain at the top surface is compressive: $\epsilon_f < 0$, and the shrinkage strain at the top surface is tensile: $\epsilon_s > 0$. The combined

strain at the top surface ϵ_{top} is the sum of the two.

$$\epsilon_{top} = \epsilon_{sh} - \frac{f_c}{E_c} \tag{39}$$

The value of ϵ_{top} is shown in Fig. 7 as a function of the reinforcement ratio p. Over the range of possible values of p, the strain in the top surface appears to be negative. In addition, the expected compressive strain is greater than 300 μm/m. Therefore, the top surface will most likely be in compression, closing off all drying shrinkage cracks.

6.8.4 Implementing the Cracking Models

Proceeding further with the analysis requires employing the specific models for cracking under flexural and shrinkage stresses. At first, the models are applied to the design independent of one another. The models will yield an estimate of the distances between cracks that will be used to combine the models.

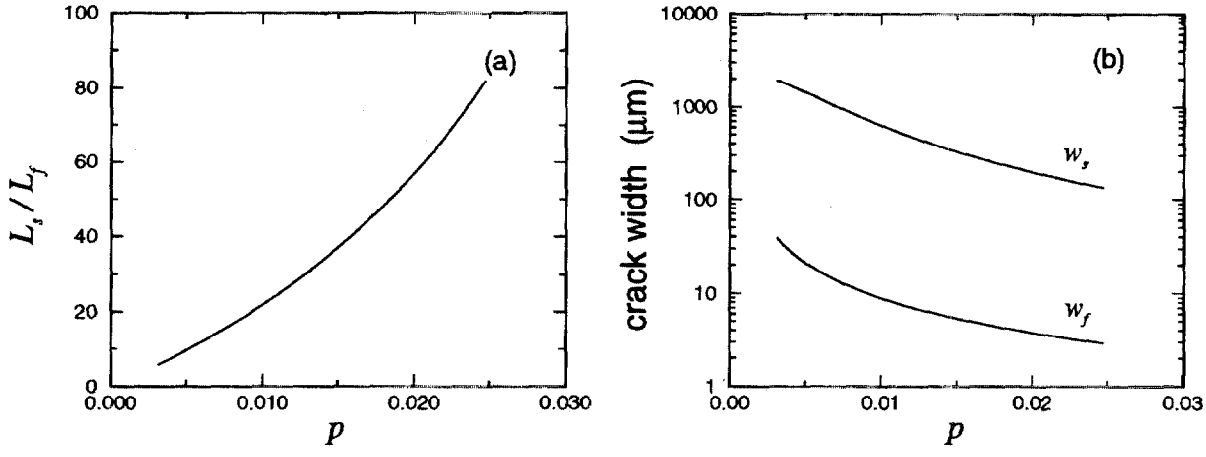

Figure 8: Results of the cracking model: (a) The ratio of the shrinkage crack spacing L_s and the flexural crack spacing L_f; (b) Flexural crack width w_f and shrinkage crack width w_s.

The estimate for the ratio of shrinkage crack spacing L_s to the flexural crack spacing L_f is shown in Fig. 8(a) as a function of the reinforcement ratio p. Over most of the allowable range for p, the ratio L_s/L_f is greater than five. Therefore, the flexural cracks will develop between shrinkage cracks.

An independent analysis of the shrinkage crack width w_s and flexural crack width w_f are shown in Fig. 8(b) as a function of the reinforcement ratio p. From an assessment of the estimate of crack widths, the combined crack widths will certainly be tens, if not

hundreds, of micrometers wide. The cracks will occur at the tension face and extend at least to the neutral axis.

6.9 Composite Permeability

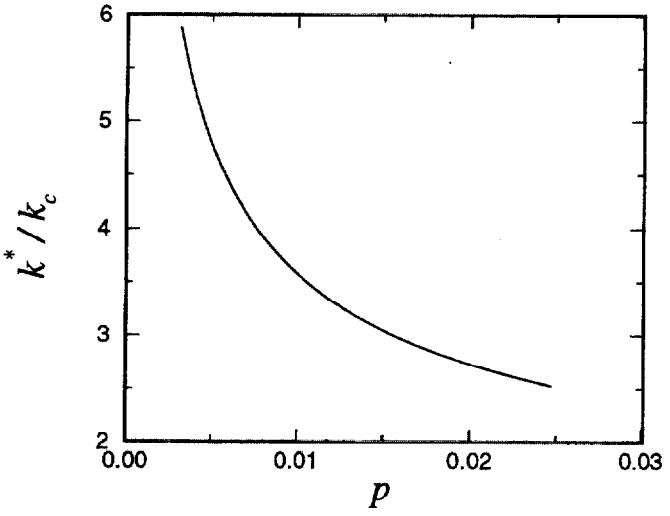

Figure 9: Ratio of the composite permeability k^* to the uncracked concrete permeability k_c as a function of reinforcement ratio p.

Since the permeability of the cracked portion of the slab will be orders of magnitude greater than the uncracked portion of the concrete, further analysis can be simplified by approximating the composite permeability k^* using Eqn. 5:

$$\frac{k^*}{k_c} \approx \alpha^{-1} = \frac{h}{\lambda d}$$

This result is plotted in Fig. 9 as a function of the reinforcement ratio p. The ratio of the permeabilities increases by less than a factor of five over most of the allowable range of p.

7 Probabilistic Approach

The previous deterministic analysis is useful for establishing what designs should work from a structural perspective. However, a probabilistic analysis is required for determining the effects of variability among the input parameters.

7.1 Initial Material Parameters

The following probabilistic analysis follows identically from the previous section with the only exception being that some of the input parameters are normally distributed about some mean value with a coefficient of variation (CoV) (the ratio of the mean to the standard deviation). The parameters allowed to vary are shown in Table 2. Note that the mean values are identical to the previous deterministic analysis.

Table 2: The mean and associated coefficient of variation (CoV) for the input parameters that would be used in an uncertainty analysis of flexural and shrinkage cracking.

Variable	Property	Mean	CoV
L	Slab length (m)	10.0	0.05
E_c	Concrete Modulus (GPa)	28.6	0.05
f'_c	Concrete compressive strength (MPa)	35.0	0.05
h	Slab thickness (m)	1.00	0.10
d	Depth of steel (m)	0.90	0.05
ϵ_s	Shrinkage strain (μm/m)	90	0.25

The values for the coefficient of variation given in Table 2 are not based on any particular data. Rather, they are values that appear reasonable. An analysis of particular vault should be done with careful consideration of the construction plans. For example, the CoV for the slab thickness given above is large compared to normal slab on grade construction. The reason for this is the assumption that the contents of the vault would be compacted remotely, and so the variability of the slab thickness would be greater than for normal practices. Construction plans for specific vaults may vary and warrant a smaller CoV.

For the probabilistic analysis, the randomization is done as a function of the reinforcement ratio p. For each value of p, random values are drawn for the parameters shown above. Using these, the analysis proceeds as for the deterministic analysis. The approach used by `4sight` would be to establish a fixed reinforcement ratio p and then repeat the analysis at a constant value of p, randomizing the input parameters listed above. `4sight` would then report the mean and standard deviation of the results at a given reinforcement ratio.

7.2 Results

The material and structural parameters given in Table 2 are used to recalculate the same quantities as were calculated for the deterministic analysis. The only difference is that the calculation is repeated many times. Each time, a value for the reinforcement ratio p is chosen and then the computer generates a random number for each parameter listed

in Table 2. This "randomized" value is then used in the deterministic analysis. The variation in the result indicates the output sensitivity to that parameter, at that value of CoV. In addition, included in each figure is a solid curve indicating the values from the previous deterministic calculations.

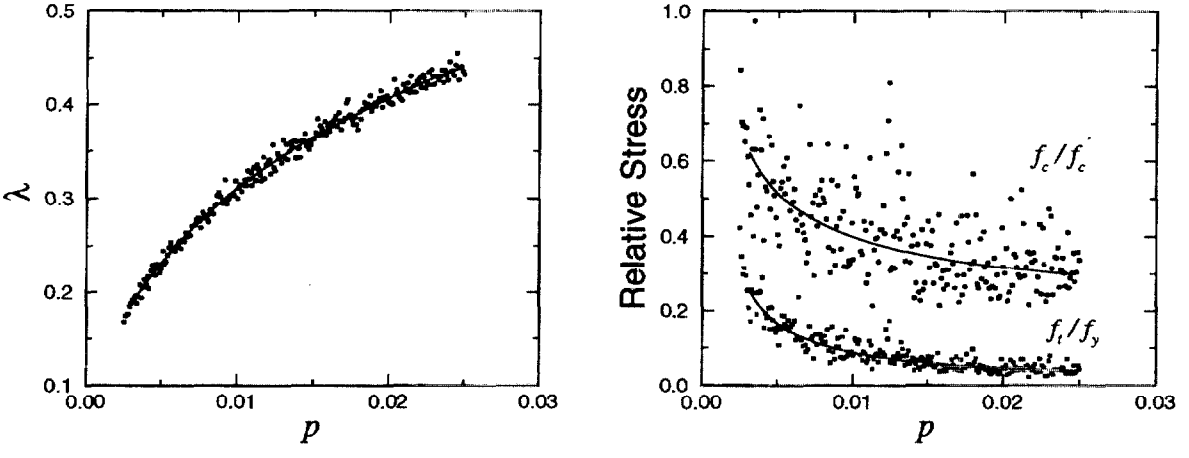

Figure 10: Analysis results: (a) Relative depth of neutral axis λ; (b) Relative tensile stress f_t/f_y and compressive stress f_c/f_c' for the cracked section analysis.

The results for the depth of the neutral axis and the relative strains are shown in Fig. 10 and can be compared directly to Fig. 6. In general, the probabilistic data follow the same trends as in the deterministic case. The calculated depth of the neutral axis shown in Fig. 10(a) are a function of the reinforcement ratio p. The results indicate that the uncertainty in the depth of the neutral axis is relatively insensitive to the uncertainty in the input parameters.

By comparison, the relative compressive and tensile stresses shown in Fig. 10(b) are much more sensitive. The variability in the compressive stress ratio f_c/f_c' is dramatic, with some of the values approaching one, even for relatively large reinforcement ratios. The number of large ratios of f_c/f_c' are in indication of the likelihood for the top surface of the concrete to experience compressive failure.

The estimated strain in the top surface of the concrete, for two values of the ultimate shrinkage strain ϵ_{sh} is shown in Fig. 11. The corresponding deterministic calculation is denoted by the solid curve. The data indicate that for all values of reinforcement ratio p the expected strain ϵ_{top} in the top surface of the vault is less than zero. Therefore, the top surface should be under a compressive strain of at least 200 μm/m.

The ratio of the shrinkage crack spacing L_s to the flexural crack spacing L_f is shown in Fig. 12(a) as a function of the reinforcement ratio p. Although the ratio has large variation, the value is typically far greater than one. Therefore, regardless of the variation

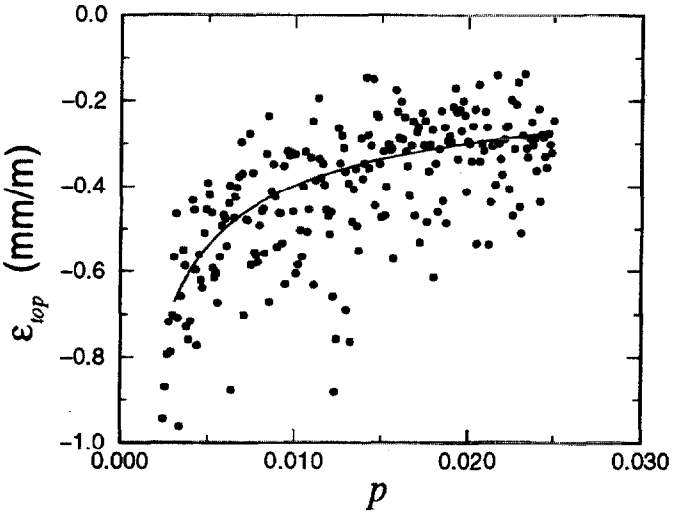

Figure 11: Strain in top surface ϵ_{top} of the slab for an ultimate drying shrinkage strain ϵ_{sh} of 90 μm/m.

in input parameters, one expects that flexural cracks will be initiated between the existing shrinkage cracks.

The shrinkage crack width w_s and flexural crack width w_f are shown in Fig. 12(b). The problematic shrinkage crack widths seem to be insensitive to the variations in the input parameters. Although the flexural cracks appear to be more sensitive, the data are plotted on a logarithmic ordinate which enhances the appearance of variability in smaller quantities.

Since the expected crack widths are still on the order of tens or hundreds of micrometers, the estimate of the bulk concrete permeability k^* can again be simplified with the following approximation:

$$\frac{k^*}{k_c} \approx \frac{h}{\lambda d}$$

This result is shown in Fig. 13. Since the depth of the neutral axis was fairly insensitive to the variability of the input parameters, the relative bulk permeability is also relatively insensitive to parameter variation. The added variation over λ is due to the variability in the roof thickness h and the depth of steel reinforcement d.

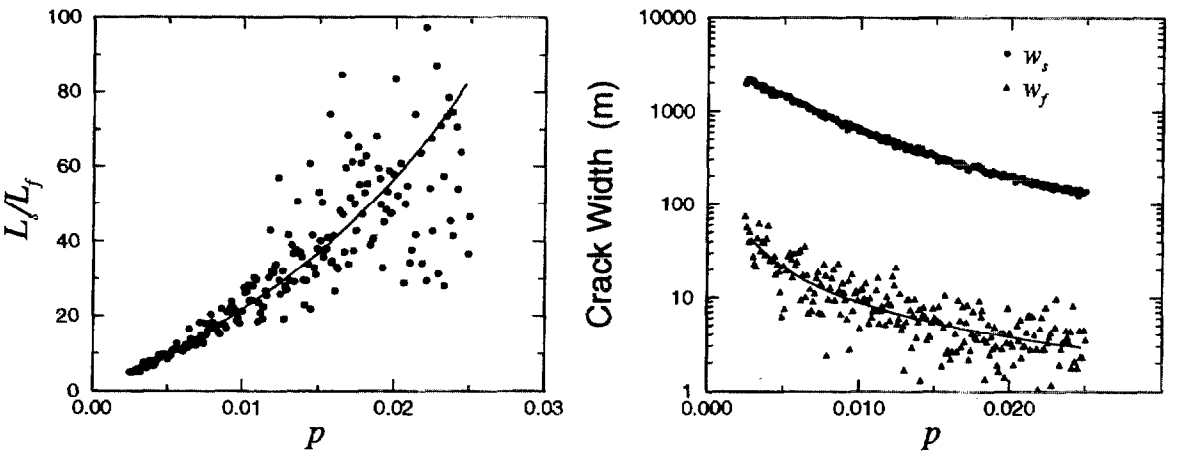

Figure 12: Results of the cracking model: (a) The ratio of the shrinkage crack spacing L_s and the flexural crack spacing L_f; (b) Flexural crack width w_f and shrinkage crack width w_s.

8 Implementation

The analysis demonstrated in the probabilistic calculation forms a basis for the calculations performed by `4sight`. Ideally, the flexural and shrinkage crack widths and spacings will be supplied by the user, based upon a careful structural analysis. In those cases where this information cannot be provided by the user, `4sight` will attempt to assist the user in estimating these quantities. To this end, there will exist two general levels of analysis. In a Level I analysis by `4sight`, the user has already performed a structural analysis. In a Level II analysis `4sight` will, with as much information as is available from the user, perform a structural analysis as outlined in this report.

8.1 Level I Analysis

The required information from the user in order to perform a Level I analysis is shown in Table 3, along with its associated variable. The depth of the neutral axis is calculated from the product of the reinforcement depth d and the neutral axis parameter parameter λ. This level of analysis assumes that the user has ensured that the concrete above the neutral axis is in compression.

From the data in Table 3, `4sight` calculates the roof composite permeability from Eqn. 5. From the coefficient of variation for each parameter, `4sight` uses computer-generated random numbers to predict probabilistic values for the user-desired output quantities; for a deterministic calculation, the user can specify values of zero for each coefficient of variation. The probabilistic calculations can be repeated internally by

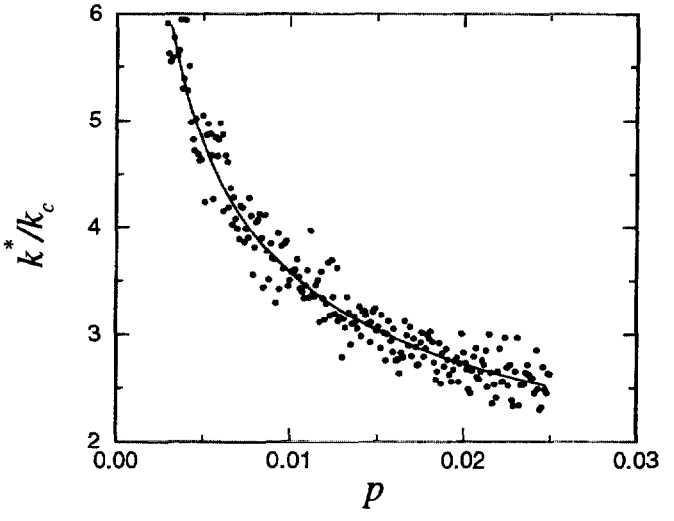

Figure 13: Ratio of the composite permeability k^* to the uncracked concrete permeability k_c: $k^*/k_c \approx \lambda^{-1}$.

4sight, and the resulting average and standard deviation of the output reported back to the user.

8.2 Level II Analysis

The required information from the user in order to perform a Level II analysis is shown in Table 4, along with its associated variable. These quantities are the same as those shown in Table 2. From these data, 4sight will perform a structural analysis identical to the one performed for the data in Table 2; a one-way slab design based upon the shorter of the two span lengths. In cases where the two span lengths are approximately equal, a one-way design based on the shorter length will be a conservative approximation since the resulting calculated stresses will be greater than for a two-way analysis of the same dimensions.

The information given in Table 4 will be used to calculated the mean and standard deviation of the quantities shown in Table 3. These quantities will then go onto a 4sight degradation calculation as in the case for a Level I analysis.

8.3 4sight Outputs

The modifications to 4sight will include the option of performing probabilistic calculations for the entire degradation calculation. Not only will the structural information

Table 3: Parameters for which a mean and standard deviation are to be supplied by the user for a Level I analysis.

Level I

User Inputs	Variable
Roof width	L
Roof thickness	h
Depth of steel reinforcement	d
Reinforcement ratio	p
Flexural crack spacing	L_f
Flexural crack width	w_f
Shrinkage crack spacing	L_s
Shrinkage crack width	w_s
Neutral axis depth parameter	λ

given in Table 3 have uncertainties, but also all the other possible input parameters such as material properties and environmental conditions. At the request of the user, `4sight` will perform multiple calculations of a given scenario and report the mean and standard deviation of desired output quantities such as service life, depth of ionic species penetration, depth of sulfate attack, etc.

9 Summary

Models for both drying shrinkage and flexural cracking have been applied to a structural analysis of a concrete vault roof. The results from the model indicated that the crack widths would be tens or hundreds of micrometers. Since the permeability of such cracks is orders of magnitude greater than that of the uncracked concrete, the control of the bulk permeability is a matter of controlling the depth of the structural neutral axis. For a steel reinforcement depth of d, and a neutral axis depth expressed as the product $\lambda\, d$, the ratio of the bulk permeability to the uncracked permeability is nearly λ^{-1}.

The analysis was repeated using a probabilistic approach. The input parameters were allowed to vary about a mean value, and the corresponding results of the analysis were recorded. The response variability reflected the sensitivity to the parameter variability. Although crack width was sensitive to input variability, the depth of the neutral axis, and hence the bulk permeability, was relatively insensitive to variability in the input parameters.

The probabilistic approach demonstrated here will be incorporated into the `4sight`

Table 4: Parameters for which a mean and standard deviation are to be supplied by the user for a Level II analysis.

Level II

User Inputs	Variable
Shorter roof span	L
Roof thickness	h
Depth of steel reinforcement	d
Reinforcement ratio	p
Concrete modulus	E_c
Concrete compressive strength	f_c'
Ultimate drying shrinkage strain	ϵ_s

computer program. The average results reported by `4sight` will give the user an indication of those parameters that have the greatest effect on the estimated permeability. The uncertainties reported by `4sight` not only indicate the output variability, but the uncertainties will also assist the user in determining the maximum allowable parameter uncertainties in order to maintain a given level of confidence in the concrete performance.

Appendix

A Poiseuille Flow in Cracks

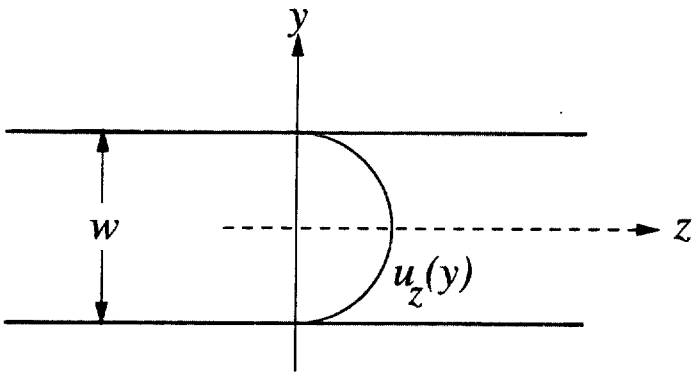

Figure 14: Poiseuille flow in the direction z through a crack of width w.

For completeness, it will be instructive to show how to calculate the permeability of smooth parallel plates separated by a distance w. Since the relevant crack widths in concrete are many times the size of water molecules, one can take a continuum approach to solving the Stokes equation. From the total flow through the plates for a given hydraulic pressure gradient, one can calculate the corresponding permeability coefficient.

The schematic of the physical system shown in Fig. 14 is composed of two plane, parallel plates separated by a distance w. The y-direction is normal to the plane surface, and the water is moving in the z-direction. For low Reynolds number, a conservation of momentum gives the Stokes equation:

$$\nabla^2 \mathbf{u} = \frac{1}{\mu} \nabla P \tag{40}$$

A conservation of mass leads to the continuity equation:

$$\frac{\partial \rho}{\partial t} + \nabla \cdot (\rho \mathbf{u}) = 0 \tag{41}$$

From these two equations, and physical arguments, one can demonstrate that the only quantity of relevance is the z-component of the velocity as a function of y:

$$\frac{\partial^2 u_z}{\partial y^2} = \frac{\partial P / \partial z}{\mu} \tag{42}$$

This second order equation requires two boundary conditions. The first is that the velocity is zero at a surface. The second boundary condition comes from the symmetry of the system:

$$\left.\frac{\partial \mathrm{u}}{\partial y}\right|_{y=0} = 0 \tag{43}$$

The complete solution to the differential equation is determined from satisfying the first boundary condition:

$$u_z = \frac{\partial P/\partial z}{2\mu} y^2 + C \tag{44}$$

$$= \frac{\partial P/\partial z}{2\mu}\left[y^2 - \left(\frac{w}{2}\right)^2\right] \tag{45}$$

The second boundary condition is satisfied by the absence of a linear term in Eqn. 44. The pressure gradient $\partial P/\partial z$ is just a parameter of the problem and is treated like a constant here, noting that flow is in the direction of the negative pressure gradient.

The permeability coefficient is defined from the average flow across the crack:

$$\langle u_z \rangle = \frac{-k}{\mu} \nabla P \tag{46}$$

The average velocity is the integrated average:

$$\langle u_z \rangle = \frac{1}{w} \int_{-w/2}^{+w/2} u_z(y)\, dy \tag{47}$$

$$= \frac{-w^2}{12\mu} \frac{\partial P}{\partial z} \tag{48}$$

By comparison to Darcy's law, the permeability of the crack is the coefficient of this equation that corresponds to the permeability term:

$$k_c = \frac{w^2}{12} \tag{49}$$

References

[1] K.A. Snyder, "Review and Partial Validation of the 4SIGHT Computer Model," *NISTIR-xxx*, National Institute of Standards and Technology, 1999.

[2] K.A. Snyder and J.R. Clifton, "4SIGHT Manual: A computer program for modeling degradation of underground low level waste concrete vaults," *NISTIR 5612*, National Institute of Standards and Technology, 1995.

[3] A.H. Nilson and G. Winter, *Design of Concrete Structures* (Tenth Edition), McGraw-Hill, 1986.

[4] *ACI Manual of Practice*, American Concrete Institute, 1998.

[5] G.D. Base and M.H. Murray, "A new look at shrinkage cracking," *Civil Engineering Transactions* (Australia) **CE 18**, No. 2, 171–176, 1982.